

# Exploring massive star early evolution: the case of the Herschel 36 A triple system

Julia I. Arias,<sup>1★</sup> Gonzalo Holgado<sup>2</sup>,<sup>2★</sup> Roberto Gamen<sup>3,4★</sup>, Nidia I. Morrell<sup>5</sup> and Abdo R. Campillay<sup>1</sup>

<sup>1</sup>*Departamento de Astronomía, Universidad de La Serena, Av. Juan Cisternas 1200 Norte, La Serena, Chile*

<sup>2</sup>*Instituto de Astrofísica de Canarias, E-38200 La Laguna, Tenerife, Spain*

<sup>3</sup>*Instituto de Astrofísica de La Plata, CONICET-UNLP, Paseo del Bosque s/n, B1900FWA, La Plata, Argentina*

<sup>4</sup>*Facultad de Ciencias Astronómicas y Geofísicas, UNLP, Paseo del Bosque s/n, B1900FWA, La Plata, Argentina*

<sup>5</sup>*Las Campanas Observatory, Carnegie Observatories, Casilla 601, La Serena, Chile*

Accepted 2024 October 8. Received 2024 October 8; in original form 2023 August 25

## ABSTRACT

Theoretical models show that some massive stars have not yet arrived at the zero-age main sequence (ZAMS) at the end of the accretion phase. At that time, they have lost their thick envelopes and thus could be optically visible. Although some candidates to optically observable ZAMS stars have been reported, the evolutionary status of none of them has been confirmed yet. The O-type triple system Herschel 36 A (H36A) is one of these candidates. We present the quantitative spectral analysis of the individual stellar components of H36A and investigate the evolutionary status of the system by contrasting main-sequence and pre-main-sequence models. Overall, the derived parameters suggest that the components of H36A could be pre-main-sequence stars going through the very last contraction to the ZAMS. However, the possibility of them already being on the main sequence is not yet ruled out. This study highlights the importance of considering multiple evolutionary models and shows that H36A represents a key object for understanding massive star formation and early evolution.

**Key words:** stars: binaries: close – stars: binaries: spectroscopic – stars: individual: Herschel 36 – stars: massive.

## 1 INTRODUCTION

Massive stars, i.e. those bearing more than  $8 M_{\odot}$ , are key objects to understand the Universe. Our knowledge of their formation, a process occurring in distant and obscured regions, is still incomplete. Two different mechanisms have been proposed for the formation of massive single stars: accretion growth and merger events (see Krumholz 2015 and references therein). In the former scenario, an initially lower mass star accretes material from the surroundings and grows to become massive (e.g. Kratter et al. 2008, 2010). In the latter, two or more intermediate-mass stars merge to produce a more massive object (e.g. Clarke & Bonnell 2008; Moeckel & Clarke 2011).

Multiplicity is a central characteristic of high-mass stars. They have been shown to have companions from the earliest main-sequence (MS) phases. An explanation relies on the tendency of the accretion discs that feed massive protostars to fragment due to gravitational instability (Kratter, Matzner & Krumholz 2008; Kratter 2012). Current high angular observations of massive protobinaries at scales of hundreds of astronomical units (au) support this scenario (e.g. Zhang et al. 2019). In recent years, considerable effort has been devoted to understand the precise mechanism by which massive binaries are formed (Meyer et al. 2018; Moe & Kratter 2018). However, many questions remain open, especially regarding the formation of close systems (with separations smaller than 10 au)

for which other processes (such as clump migration, evolution, etc.) may take place in addition to disc fragmentation.

At present there is no convincing evidence against the idea that massive stars form via the same accretion mechanisms that give rise to low-mass stars. Current models considering the major difficulties in forming massive stars, i.e. fragmentation, radiation pressure, photoionization, and stellar winds, show that neither mechanism is apparently capable of halting the growth of stars by accretion (Krumholz 2015 and references therein). One of the certainties of the formation of massive stars by accretion is the rapid time-scale for the evolution of the protostars, a consequence of the high accretion rates involved in the process. Accretion rates of  $\dot{M}_{\star} \sim 10^{-4} M_{\odot} \text{ yr}^{-1}$  are necessary to allow continuing accretion on to an O star (e.g. Kuiper & Yorke 2013.; Kuiper & Hosokawa 2018).

Theoretical models (e.g. Hosokawa & Omukai 2009) distinguish a variety of evolutionary stages of single massive protostars. First, an adiabatic accretion phase, followed by a ‘swelling phase’ in which the protostellar radius becomes very large, eventually exceeding  $100 R_{\odot}$ . Observational evidence of such ‘bloated’ stars is still scarce but growing (Ochsendorf et al. 2011; Palau et al. 2013). At a certain mass value that depends on the model, the protostar turns to contraction, losing heat with a thermal Kelvin–Helmholtz (KH) time-scale  $t_{\text{KH}}$ . During this so-called KH contraction phase, the interior temperature increases gradually until it finally reaches  $10^7$  K and the nuclear fusion of hydrogen begins. Once the nuclear burning energy is sufficient to balance the radiative losses, the contraction stops and the star reaches the zero-age main-sequence (ZAMS) phase.

\* E-mail: [jarias@userena.cl](mailto:jarias@userena.cl) (JIA); [gonzalo.holgado@iac.es](mailto:gonzalo.holgado@iac.es) (GH); [rgamen@fcaglp.unlp.edu.ar](mailto:rgamen@fcaglp.unlp.edu.ar) (RG)

For years it was stated that massive stars begin core hydrogen burning while still accreting deeply embedded within their parental molecular clouds (Yorke 1986) and, consequently pre-main-sequence (PMS) massive stars were impossible to observe in the optical range. In this scenario, optically visible O stars, which lack thick dusty envelopes, had to be already somewhat evolved. The paradigm has recently changed thanks to the latest theoretical models which show that, if high accretion rates are achieved, stars as massive as  $\sim 15 M_{\odot}$  have not yet reached the ZAMS at the end of the accretion phase (Hosokawa & Omukai 2009). These PMS massive stars are very luminous and have effective temperatures much lower than a ZAMS star of equal mass. Because much of the surrounding absorbing material has been removed, these objects are potentially observable at optical wavelengths during the KH contraction phase. However, the very short time-scale that governs these ‘last steps’ in their way to the ZAMS ( $t_{\text{KH}}$  falls below  $10^4$  yr for stars with masses  $> 10 M_{\odot}$ ; Hosokawa & Omukai 2009) critically limits the possibility of detecting them.

The dearth of massive stars near the ZAMS has been a long-standing topic of discussion. Based on the spectroscopic analysis of a large unbiased sample of Galactic O-type stars, Holgado et al. (2020) confirmed the apparent lack of ZAMS objects in the mass range of  $\approx 30 - 70 M_{\odot}$ . Similarly, Schootemeijer et al. (2021), combining spectral types from catalogues with *Gaia* magnitudes, reported a dearth of young and bright massive stars in the Small Magellanic Cloud. For 30 Doradus in the Large Magellanic Cloud, although the location near the ZAMS is well populated, Schneider et al. (2018) reported a lack of stars younger than  $\approx 1$  Myr among the OB stars from the spectroscopic VFTS. This fact is evidenced by a sparsely occupied region in the Hertzsprung–Russell diagram (HRD) between the ZAMS, the 1 Myr isochrone, and the  $30 M_{\odot}$  stellar track. In spite of the former, various optical O stars have been pointed out as extremely young objects, likely on or very near to the ZAMS. For example, Walborn (2009) presents a nice compilation of optically observable ZAMS O candidates in both the Galaxy and the Magellanic Clouds. The actual evolutionary status of most of them remains unclear.

This paper is the second part of a study devoted to Herschel 36 A (H36A), a conspicuous ZAMS candidate star (Walborn 2009) in the heart of the Lagoon nebula. The extreme youth of this object is claimed on the basis of different observational features, for example, its association with dense, dusty nebular knots, the presence of an infrared star cluster around it (Arias et al. 2006), and the Vz nature of its optical spectrum. While the Vz classification has historically been linked to stellar youth, Sabín-Sanjulián et al. (2014) showed that this is not necessarily the case in low-metallicity environments like 30 Doradus, where the modest O-star winds might cause this spectral feature to persist for a longer period. However, in the Galaxy, Arias et al. (2016) demonstrated that almost all O Vz stars are associated with very young clusters (ages less than 3 Myr), supporting the interpretation of the Vz characteristic as a signature of youth in higher metallicity environments. In a previous paper (Campillay et al. 2019, hereafter Paper I), we confirmed that H36A is a hierarchical system, composed of a very close OB binary (Herschel 36 Ab1, Ab2) in a wide orbit around a third O-type star (Herschel 36 Aa), and we used a spectral disentangling method to obtain the individual spectra of the three stellar components. We also calculated high-precision spectroscopic solutions for the inner and outer orbits, i.e. the orbits corresponding to the movement of the close pair, and to the movement of the stars around the centre of mass of the triple system, respectively.

In this paper, we advance in the physical characterization of the H36A system by performing the quantitative spectroscopic analysis of its three stellar components. The observational material on which the study is based is described in Section 2. In Section 3, we present the details of the quantitative spectroscopic method, along with the obtained results. We discuss these results in Section 4 and we summarize the main findings and conclusions in Section 5.

## 2 OBSERVATIONAL MATERIAL

The spectroscopic study presented here is based on the individual spectra of the three stellar components of H36A obtained in Paper I by applying a spectral disentangling method (González & Levato 2006) to the observed composite spectra of the system. The observed data are part of the OWN Survey (Barbá et al. 2010, 2017), a high-resolution spectroscopic monitoring of O- and WN-type stars started in 2005, which uses facilities in Chile and Argentina. The reader is referred to Paper I for details of the instrumental configurations, data processing, and application of the disentangling method. In short, the triple disentangling method is an iterative process that uses alternately the spectrum of one component to calculate the spectra of the others. It was achieved using 24 high-quality (S/N  $\approx 150$ ), high-resolution ( $R \approx 48\,000$ ) FEROS spectra<sup>1</sup> (ESO/La Silla Observatory), covering a wavelength range of 3900 – 5000 Å. As a result, it was found that the stars Aa, Ab1, and Ab2 contribute to the global spectrum by 46 per cent, 38 per cent, and 16 per cent (with an uncertainty of about 2 per cent), respectively. These factors were used to re-scale the spectra to account for the dilution effect. Fig. 1 shows the reconstructed spectra for the three stellar components. The signal-to-noise ratio (SNR) of the reconstructed spectra, measured near 4800 Å, is 280, 230, and 130 for Aa, Ab1, and Ab2, respectively.

## 3 RESULTS OF THE QUANTITATIVE SPECTROSCOPIC ANALYSIS

The spectroscopic quantitative analysis of the three components of H36A was performed using the IACOB Grid-Based Automatic Tool (IACOB-GBAT, (Simón-Díaz et al. 2011)). IACOB-GBAT uses a large grid of precomputed FASTWIND stellar atmosphere models (Santolaya-Rey, Puls & Herrero 1997; Puls et al. 2005) to compare the observed and synthetic profiles of selected H and He lines. From the comparison, a number of photospheric and wind parameters can be derived. Solar metallicity ( $Z = Z_{\odot}$ ) models were adopted in the analysis. The H and He lines considered are listed in Table 1.

### 3.1 Line broadening

The analysis with IACOB-GBAT requires as input the line-broadening parameters that characterize the spectrum. To estimate them we used the IACOB-BROAD (Simón-Díaz & Herrero 2014), another semi-automated tool that combines the Fourier Transform and the Goodness-Of-Fit techniques to characterize the broadening of the selected spectral lines. The program allows to disentangle the rotational ( $v \sin i$ ) and macroturbulent ( $v_{\text{mac}}$ ) contributions to the line profiles.

<sup>1</sup>ESO program identifications: 077.B-0348(A), 079.D-0564(A), 081.D-2008(A), 081.D-2008(B), 083.D-0589(A), and 089.D-0975(A).

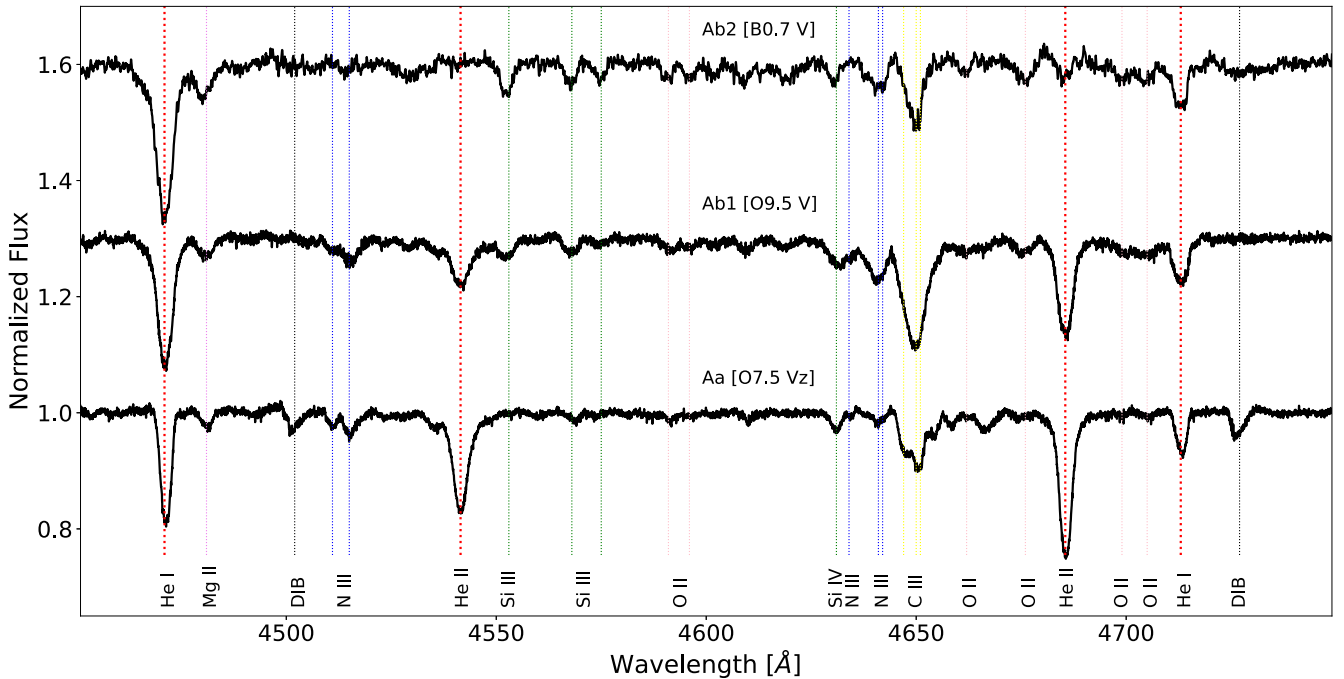


**Figure 1.** Normalized spectra of the three stellar components of H36A obtained from the disentangling of the observed composite spectrum. The templates have been scaled to account for the dilution effect. Important spectral lines and some diffuse interstellar bands are identified.

**Table 1.** Hydrogen and helium lines used in the quantitative spectroscopic analysis.

H I	He I	He II	He I + II
H $\epsilon$	4388	4200	4026
H $\delta$	4471	4542	
H $\gamma$	4713	4686	
H $\beta$	4922		

For each stellar component, several metallic and He I lines were studied. Since helium lines are influenced by Stark broadening, the final results were obtained by averaging measurements from both helium and metallic lines to produce a single value. For the uncertainties of  $v \sin i$ , we adopted 10 per cent of the central value, as obtained by the authors of IACOB-BROAD for the Galactic O-type star sample in Holgado et al. (2022), and the standard deviation for the used lines for  $v_{\text{mac}}$ . The line profiles become dominated by rotation when projected rotational velocities exceed  $100 \text{ km s}^{-1}$ ; however, both  $v \sin i$  and  $v_{\text{mac}}$ , and its error distribution, are being considered for the spectroscopic analysis. Table 2 shows the studied spectral lines, along with the final values of  $v \sin i$  and  $v_{\text{mac}}$ , and their errors.

The broadening parameters were determined from the templates resulting from the spectral disentangling process, each one being a sort of mean spectrum obtained from the average of the various input spectra, weighted by their SNR and their distribution along the orbital cycle. In particular, it is likely that the binary components of the close pair Ab1 and Ab2 are distorted by tidal interactions, showing therefore different spectra at different orbital phases. Due to this fact, together with other caveats that will be discussed in Section 4, some caution is necessary in the interpretation of these values.

### 3.2 Photospheric and wind parameters

The following atmospheric parameters were derived for each stellar component: effective temperature  $T_{\text{eff}}$ , surface gravity  $\log g$ , abundance of helium relative to hydrogen  $Y_{\text{He}}$ , microturbulence  $\xi_T$ , and the wind-strength  $Q$ -parameter.<sup>2</sup> In this case, the  $\beta$  exponent of the wind velocity law was fixed to 1.0. Figs 2, 3, and 4 illustrate the results for the Aa, Ab1, and Ab2 components, respectively. The coloured spectrum is the stellar component template, while the black line represents the best-fitting model. The considered and discarded points in the fit of each diagnostic line are indicated in red and blue, respectively. The obtained values and their errors are presented in the second block of Table 3. The gravity corrected from rotational velocity, defined as  $\log g_c = \log [g + (v \sin i)^2 / R_*]$  (see Repolust et al. 2004), is included in this Table.

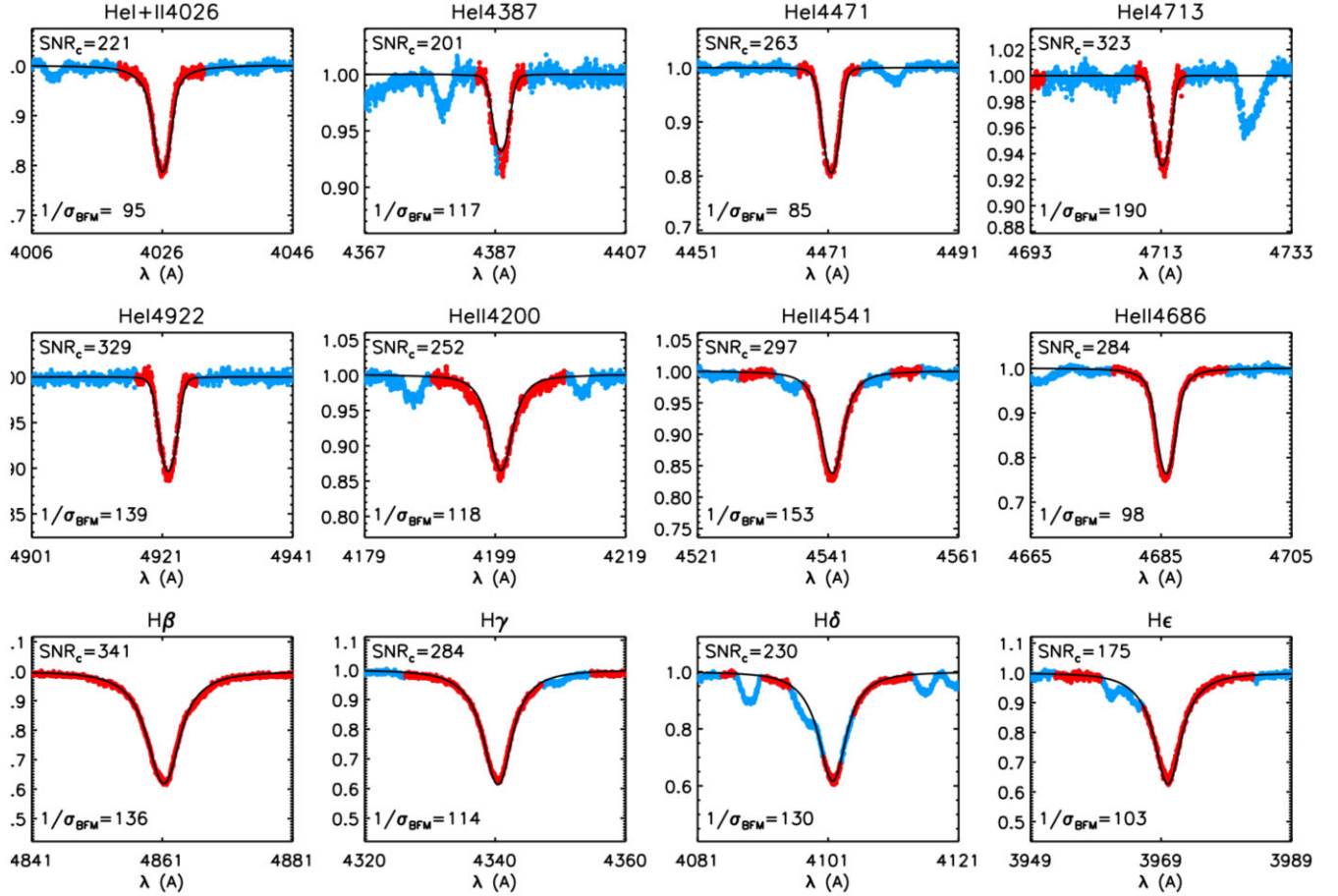
Taking into account the absence of He II lines in the cooler component (Ab2), we considered an additional method to determine a valid temperature range to supply to the IACOB-GBAT analysis. We utilized FASTWIND models to analyse the expected equivalent width of the most prominent lines of Si II, Si III, and Si IV within the studied wavelength range with the range of effective temperatures and gravities in our grid. Given that Si II and Si IV lines are absent, we infer that the temperature range for the Ab2 component lies between 20 and 26 kK. Consequently, we adjusted the  $T_{\text{eff}}$  range accordingly when examining the remaining spectroscopic parameters.

The effective temperatures and gravities derived for the components of H36A are consistent with their spectral types. Within the uncertainties, these parameters are in good agreement with the current calibrations for O stars in the Milky Way (e.g. Martins, Schaerer & Hillier 2005; Simón-Díaz et al. 2014; Holgado et al. 2018). A graphic comparison between an observed FEROS spectrum

<sup>2</sup>  $Q = \dot{M}(Rv_\infty)^{-1.5}$ , where  $\dot{M}$  is the mass-loss rate,  $R$  is the stellar radius, and  $v_\infty$  is the terminal velocity of the wind.

**Table 2.** Line broadening parameters of the components of H36A.

Component	Spectral lines	$v \sin i$ ( $\text{km s}^{-1}$ )	$v_{\text{mac}}$ ( $\text{km s}^{-1}$ )
Aa	Si IV 4116, He I 4387, N II 4630, He I 4713, He I 4922	$122 \pm 12$	$73 \pm 12$
Ab1	Si IV 4116, S III 4253, Mg II 4481, He I 4713	$173 \pm 17$	$69 \pm 17$
Ab2	S III 4253, Si III 4567, Si III 4574, O II 4590, He I 4713	$126 \pm 13$	$53 \pm 15$

**Figure 2.** Comparison between the spectral template of the component Aa and the best-fitting model for the different H and He lines used in the IACOB-GBAT analysis. See text for details.

and the best-fitting synthetic models obtained from the analysis with IACOB-GBAT is presented in Fig. 5. The green, blue, and red lines correspond to the best-fitting FASTWIND models for components Aa, Ab1, and Ab2, respectively. Individual models were added to obtain the combined spectrum represented by the black line.

### 3.3 Stellar radii, luminosities, and spectroscopic masses

Additional stellar parameters, such as the radius  $R$ , the luminosity  $L$ , and spectroscopic mass  $M_{\text{sp}}$ , can be determined with IACOB-GBAT, provided the absolute magnitude  $M_V$  is known. The absolute magnitude of each component was computed from the value  $M_V = -4.8 \pm 0.2$  corresponding to the triple system (Arias et al. 2006),<sup>3</sup>

<sup>3</sup>This value of  $M_V$  corresponds to a distance of 1250 pc, which is in excellent agreement with the distance of  $1234 \pm 16$  pc recently determined from the *Gaia* Early Data Release 3 by Maíz Apellániz et al. (2022).

using the percentages of contribution of each star to the global flux estimated in Paper I, i.e. 46 per cent for component Aa, 38 per cent for component Ab1, and 16 per cent for component Ab2. This leads to the individual absolute magnitudes quoted in the first block of Table 3.

The newest IACOB-GBAT version employs the relationship between the flux obtained from the best-fitting FASTWIND model and the  $M_V$  to calculate the radius. Starting from the model flux, the radius is adjusted until it aligns with the observed photometric data. The combination of radius and temperature is then used to obtain the luminosity. In this process, the error in  $M_V$  is propagated.

The third block of the Table 3 presents the values resulting for  $R$ ,  $\log L$ , and  $M_{\text{sp}}$ , along with their uncertainties, calculated taking into account the entire error distribution in the input parameters, and errors from the calculated intermediate parameters.

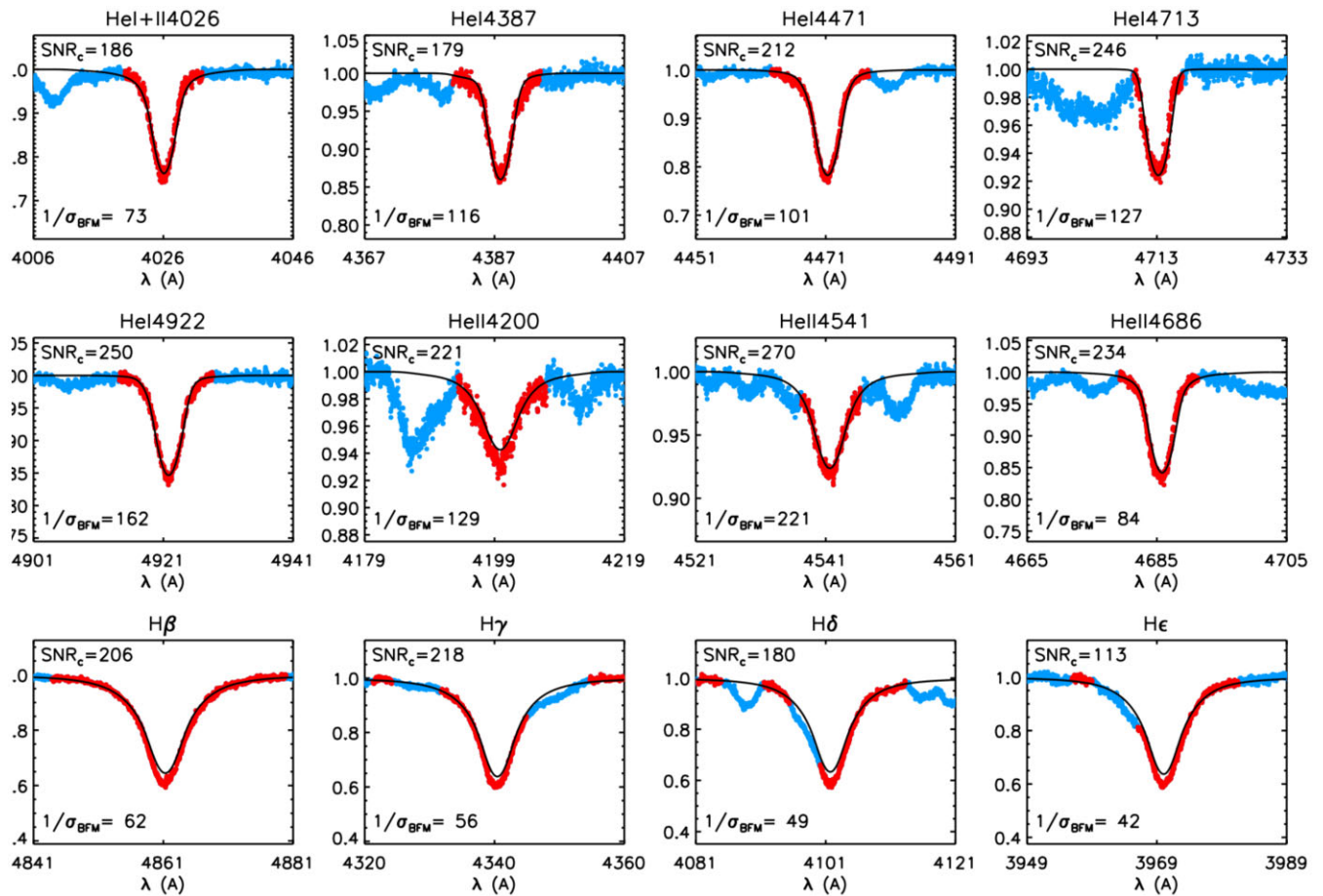


Figure 3. Same as in Fig. 2 for the spectral template of the component Ab1.

### 3.4 Comparison with evolutionary tracks

The stellar components of H36A were placed in the HRD according to the  $T_{\text{eff}}$  and  $L$  determined in the previous section. Their locations were then compared to theoretical models of stellar evolution in order to derive evolutionary masses and ages. Given the very young age proposed for H36A, we considered models representing different evolutionary stages. We ran comparisons with evolutionary models for MS stars, and two different sets for PMS evolutionary models. What follows is a description of the evolutionary properties inferred from each of the three HRDs. Some scenarios to account for the observed similarities and discrepancies will be presented in Section 4.

Fig. 6 shows the stars superimposed on the evolutionary tracks for MS single stars by Brott et al. (2011), without rotation. The ZAMS and isochrones for 1–6, 10, 13, 15, 17, and 20 Myr are also shown. Evolutionary masses of approximately 26, 20, and 9  $M_{\odot}$  are derived for components Aa, Ab1, and Ab2, respectively, in reasonable agreement with the absolute masses calculated for the system by Sanchez-Bermudez et al. (2022, for completeness, also included in the first block of Table 3). On the other hand, their locations with respect to the isochrones imply evolutionary ages of less than 1 Myr for component Aa, more than 2 Myr for Ab1, and about 17 Myr for Ab2. Even taking into account the associated errors, the age discrepancy between the two stars that form the inner binary is important. The BONNSAI tool (Schneider et al. 2014) allow us to consolidate our values, obtained by approximate comparison on the HRD, as it conducts a Bayesian study of the

physical parameters. It provides evolutionary masses and ages using the calculated observables and the position of each component in the HRD. We utilized temperature, luminosity, radius, helium abundance, and  $v \sin i$  measurements, and the corresponding results have been included in Table 3. Due to the resolution limitations of the stellar model grid, we had to increase the uncertainty associated with  $v \sin i$ . Notably, the results align perfectly with the qualitative determination made by visual inspection.

Fig. 7 displays a diagram similar to the previous one, employing evolutionary tracks for massive accreting PMS stars from Hosokawa & Omukai (2009). These tracks are calculated assuming a constant accretion rate of  $10^{-3} M_{\odot} \text{ yr}^{-1}$ . The dotted line represents the birthline, which marks the point on the HRD where a PMS star becomes visible in the optical, and mass accretion is presumed to cease. Subsequently, the star contracts towards the ZAMS at a KH time-scale, during which its luminosity remains relatively constant. Fig. 7 illustrates that, if we assume these PMS tracks to accurately represent the evolutionary stage of the H36A components, implying that the stars are still going towards the ZAMS, their evolutionary masses are estimated to be approximately 25  $M_{\odot}$  for component Aa, and 20  $M_{\odot}$  and 10  $M_{\odot}$  for components Ab1 and Ab2, respectively. These values align well with those determined from the dynamics of the triple system. In terms of time-scales, Fig. 7 indicates that the most massive star (Aa) is virtually on the ZAMS, while the inner binary components are nearing it but have not yet reached it. The symbols on each track in Fig. 7 represent the amount of time since the end of mass accretion; thus, one can roughly estimate that the

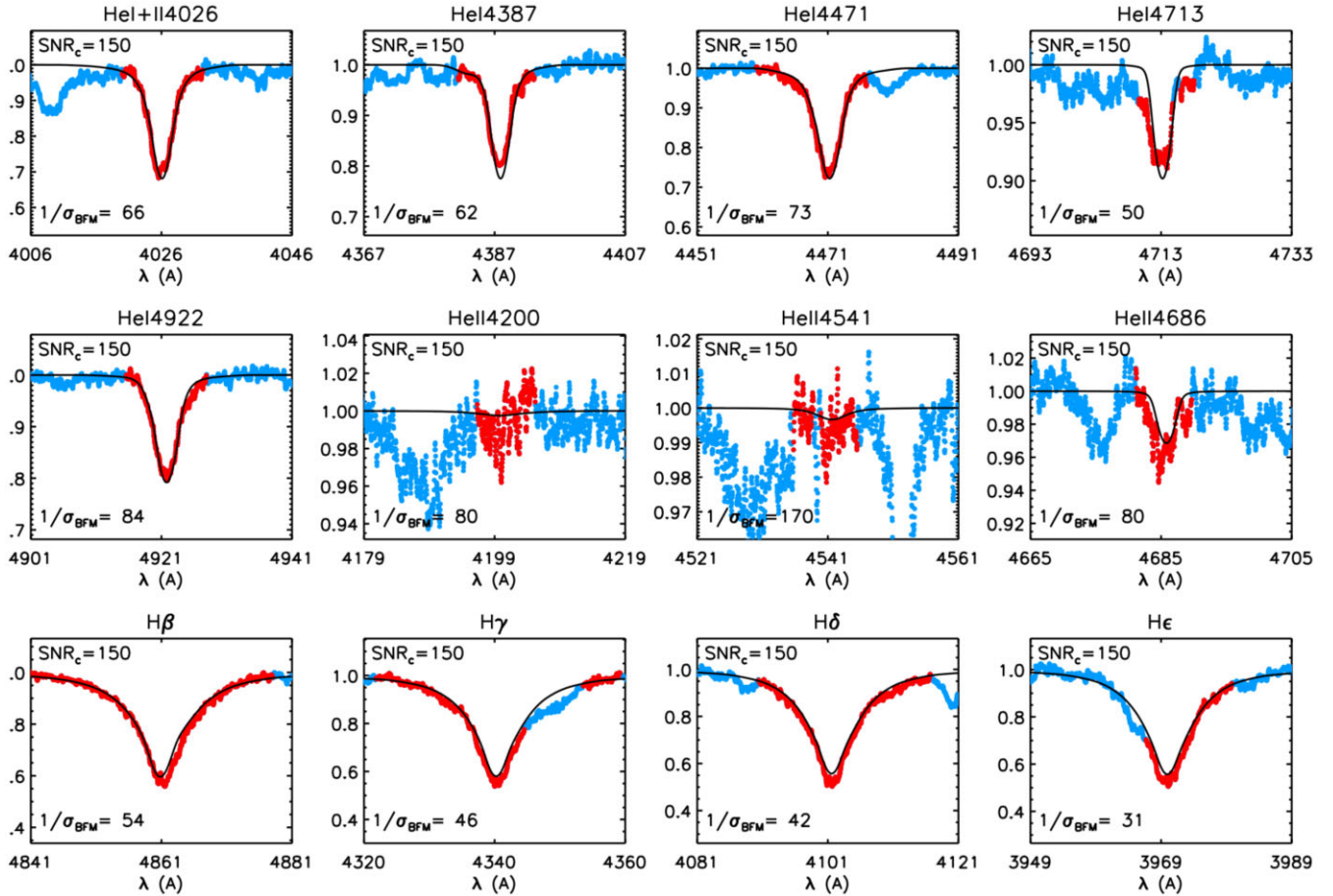


**Figure 4.** Same as in Fig. 2 for the spectral template of the component Ab2.

binary components ceased accreting mass roughly 50 000 yr ago, and it will take them a few thousand more years to reach their positions on the ZAMS.

Finally, we examined the grid of stellar models by Haemmerlé et al. (2019), which encompasses the evolution from the pre-MS accretion phase to the post-MS phase. The grid is connected with the one by Ekström et al. (2012) and is based on the same physical considerations. While it does not incorporate the effects of rotation, it offers a comprehensive overview spanning most stages of stellar evolution. The models start at a non-zero initial age of  $60.5 \times 10^3$  yr, corresponding to a  $0.7 M_{\odot}$  seed formed through accretion from  $M = 0$  at a constant rate.<sup>4</sup> This assumption was made to avoid problems in the numerical convergence and it sets an uncertainty of  $\approx 10^5$  yr in age derivation from the current grid.

Fig. 8 illustrates the H36A components within the framework of the Haemmerlé et al. (2019) models. Their overall characteristics, as inferred from their positions on the HRD, are qualitatively similar to those derived using the PMS tracks from Hosokawa & Omukai (2009). Specifically, component Aa is positioned very close to the ZAMS location expected for a  $25 M_{\odot}$  star, while components Ab1 and Ab2 are contracting towards the ZAMS on PMS tracks corresponding to approximately 19 and  $10 M_{\odot}$ , respectively. Similar to Fig. 7, symbols representing the time elapsed since the end of

mass accretion were plotted on each track. Thus, according to these models, the elapsed time since the inner-binary components stopped accreting is less than  $30 \times 10^3$  yr, and the entire KH contraction towards the ZAMS will take them less than  $100 \times 10^3$  yr. The dotted green lines in Fig. 8 denote the time since the formation of the  $0.7 M_{\odot}$  seed. Notably, the physical parameters derived for the three components of H36A place them, within the errors, between the isochrones of  $315 \times 10^3$  and  $320 \times 10^3$  yr.

The evolutionary masses and ages resulting from considering PMS models, consistent with each other, are presented in the last block of Table 3.

### 3.5 Age analysis in the mass–luminosity plane

Higgins & Vink (2023) demonstrated that the isochrone fitting method for age determination is subject to significant systematic uncertainties, primarily due to the adoption of a standardized grid of models that assume a default mixing efficiency. They utilized the mass–luminosity ( $M$ – $L$ ) plane, introduced by Higgins & Vink (2019), to develop an alternative, more reliable method for predicting stellar ages. The  $M$ – $L$  plane is a tool analogous to the HRD but it incorporates the effects of internal mixing by using models that include varying levels of overshooting and rotation, which produce distinct evolutionary tracks in the diagram. The age of individual stars is determined by fitting each observation to a theoretical model with specific parameters for convective overshooting and rotational mixing, calibrated to the observed  $T_{\text{eff}}$ , luminosity, and mass of

<sup>4</sup>The Churchwell–Henning accretion rate for  $M = 0.7 M_{\odot}$  which is  $\dot{M}_* = 1.157 \times 10^{-5} M_{\odot} \text{ yr}^{-1}$  (Behrend & Maeder 2001).

**Table 3.** Observed and derived properties of the components of H36A.

Parameter (unit)	H36Aa	H36Ab1	H36Ab2
Properties involving previous works			
Sp. type <sup>a</sup>	O7.5 Vz	O9.5 V	B0.7 V
$M_V^b$	$-3.96 \pm 0.2$	$-3.75 \pm 0.2$	$-2.81 \pm 0.2$
$M_{\text{abs}} (M_{\odot})^c$	$22.3 \pm 1.7$	$20.5 \pm 1.5$	$12.5 \pm 0.9$
Photospheric and wind parameters			
$T_{\text{eff}} (kK)$	$38.2 \pm 0.5$	$34.3 \pm 0.8$	$23.0 \pm 1.2$
$\log g$ (dex)	$3.92 \pm 0.06$	$4.01 \pm 0.17$	$3.98 \pm 0.14$
$\log g_c$ (dex)	$3.94 \pm 0.06$	$4.05 \pm 0.16$	$4.01 \pm 0.13$
$Y_{\text{He}} \times 10^2$	$11.5 \pm 1.8$	$13.7 \pm 3.0$	$12.4 \pm 2.4$
$\xi_T$ (km s <sup>-1</sup> )	< 9.0	> 20.0	< 1.0
$\log Q$ (dex)	< -13.5	> -14.0	< -13.5
Physical parameters			
$R (R_{\odot})$	$6.5 \pm 0.6$	$6.4 \pm 0.6$	$6.0 \pm 0.5$
$\log L/L_{\odot}$ (dex)	$4.91 \pm 0.08$	$4.70 \pm 0.09$	$3.94 \pm 0.12$
$M_{\text{sp}} (M_{\odot})$	$13.7 \pm 3.0$	$17.8 \pm 7.5$	$14.1 \pm 5.3$
Evolutionary parameters derived from MS models			
$M_{\text{ev}} (M_{\odot})$	$26 \pm 1$	$20 \pm 1$	$9 \pm 1$
Age (Myr)	< 1	$2 \pm 1$	$17 \pm 2.5$
Evolutionary parameters derived from MS models with BONNSAI <sup>‡2</sup>			
$M_{\text{ev}} (M_{\odot})$	$26.00^{+0.89}_{-1.01}$	$20.40^{+1.01}_{-1.03}$	$9.80^{+0.62}_{-0.75}$
Age (Myr)	$0.20^{+0.54}_{-0.19}$	$1.82^{+1.0}_{-1.14}$	$15.32^{+3.24}_{-3.05}$
Evolutionary parameters derived from PMS models			
$M_{\text{ev}} (M_{\odot})$	$25 \pm 1$	$19 \pm 1$	$10 \pm 1$
Age (10 <sup>3</sup> yr)	$315 \pm 100$	$315 \pm 100$	$315 \pm 100$

Notes.<sup>a</sup>Spectral types from Paper I.

<sup>b</sup>Computed from  $M_V = -4.8$  (Arias et al. 2006) and the contribution factors from Paper I (see Section 3.3).

<sup>c</sup>Absolute masses derived from the simultaneous fit of the available spectroscopic and interferometric data (Sánchez-Bermúdez et al. 2022).

<sup>‡2</sup>Schneider et al. (2014). The BONNSAI web-service is available at [www.astro.uni-bonn.de/stars/bonnsai](http://www.astro.uni-bonn.de/stars/bonnsai).

the star. We applied the Higgins & Vink (2023) method to the components of H36A to reproduce the system’s evolution and to determine the maximum systematic age difference that might arise from the use of the standard models discussed in the previous section.

Fig. 9 is an  $M-L$  diagram depicting the evolutionary tracks of stars with initial masses similar to those determined for the components of H36A. We consider models from the calibrated grid provided by Higgins & Vink (2019) with initial rotational velocities of 100, 200, and 300 km s<sup>-1</sup>, and two different overshooting values from the available grid ( $\alpha_{\text{ov}} = 0.1$  and  $\alpha_{\text{ov}} = 0.5$ , in brown and magenta, respectively). The diagram illustrates how different initial conditions impact the evolution of stars in this mass range. The stellar components Aa, Ab1, and Ab2 are represented by the green, blue, and red crosses, respectively.

The best estimate for the current age corresponds to the model age at which the observed effective temperature is reached at the same point where the observed mass and luminosity are also matched. In Fig. 9, small circles are marked along each model track. These circles correspond to the observed  $T_{\text{eff}}$  of the component of H36 that is closer in mass to the model. Specifically,  $T_{\text{eff}} = 38.2$  kK is indicated on the 25  $M_{\odot}$  track, 34.3 kK on the 20  $M_{\odot}$ , and 23.0 kK on both the 12 and 8  $M_{\odot}$  tracks.

Fig. 9 shows that for the two most massive stars, the effect of using standardized models is minimal. The ages inferred from the calibrated models are similar to those obtained with BONNSAI, yielding values of  $\sim 0.05$  Myr for Ab1 and  $\sim 0.01$  Myr for Aa. This similarity is reasonable because the Brott models included in BONNSAI use a core overshooting value of  $\alpha_{\text{ov}} = 0.335$ , which falls

in the middle of the range of overshooting values considered in the model grid. As a result, the largest systematic uncertainties related to core overshooting are minimized.

For the Ab2 component, using models with an initial mass of 12  $M_{\odot}$  and an initial rotational velocity of 200 km s<sup>-1</sup>, the calculated age ranges from 13.5 to 16.5 Myr, depending on the two different overshooting values in the model grid. This difference of  $\sim 3$  Myr is consistent with the maximum systematic differences of up to 3.5 Myr reported by Higgins & Vink (2023) for initial masses less than 30  $M_{\odot}$ . Notably, the age and associated uncertainty obtained are also compatible with our results from BONNSAI.

In conclusion, the analysis in the  $M-L$  plane, which accounts for systematic errors, produces age estimates for the components of H36A that are consistent with those obtained using the isochrone fitting method in the previous section.

## 4 DISCUSSION

### 4.1 Age-based arguments supporting the PMS status of Herschel 36 A

In order to study the evolutionary status of H36A, we considered theoretical models representing the MS evolution of the stars (Brott et al. 2011; Higgins & Vink 2019), but also models representing the PMS stellar evolution (Hosokawa & Omukai 2009; Haemmerlé et al. 2019). This is based on the extremely young age (less than 1 Myr) proposed for Herschel 36 and the Hourglass region, which underpins our approach. We found that the estimated evolutionary masses are more or less similar, independently of the set of models used. On the contrary, the inferred ages greatly differ and, consequently, they can be useful for distinguishing the current stage of the system’s evolution, whether it is in an MS or PMS phase.

The evolutionary ages estimated using MS theoretical models lead to a scenario which is difficult to explain. First, an age older than 2 Myr is not consistent with the extreme youth suggested for the Hourglass region on the basis of different observations. For example, the age inferred from the dynamics of the ionized gas in the region is as small as  $5 \times 10^4$  yr (Chakraborty & Anandarao 1997). Additionally, from the near-infrared photometry of a  $135 \times 139$  arcsec<sup>2</sup> area centred at the position of H36, Arias et al. (2006) concluded that the high fraction of infrared-excess sources indicates an age of about 1 Myr. Based on the Gaia-ESO Survey, Prisinzano et al. (2019) arrived at a similar conclusion: they confirmed the scenario of sequential star formation proposed for M8 (Lada et al. 1976; Damiani et al. 2004; Arias, Barbá & Morrell 2007), with the oldest stars (less than 5 Myr) distributed around the centre of the NGC 6530 cluster, and the stars in the Herschel 36 region formed only in the last 1 Myr. However, perhaps more importantly, the ages derived for the three components are irreconcilable with the current scenarios of massive star formation. In particular, the two components of the close binary, whose separation is less than 0.1 au, fall on significantly different isochrones, leading to an age difference of more than 12 Myr among them.

The formation of massive binaries is still a developing subject. Recent simulations suggest that both accretion and dynamical interactions could be important in forming binary systems. In dense clusters a dynamical three-body encounter can lead to the formation of a binary (Repolust, Puls & Herrero 2004). Although this formation channel might account for a small age difference between the binary components, such a mechanism produces very wide binaries, with a median separation of about  $10^4$  au, which is several orders larger than the separations between the three components of H36.

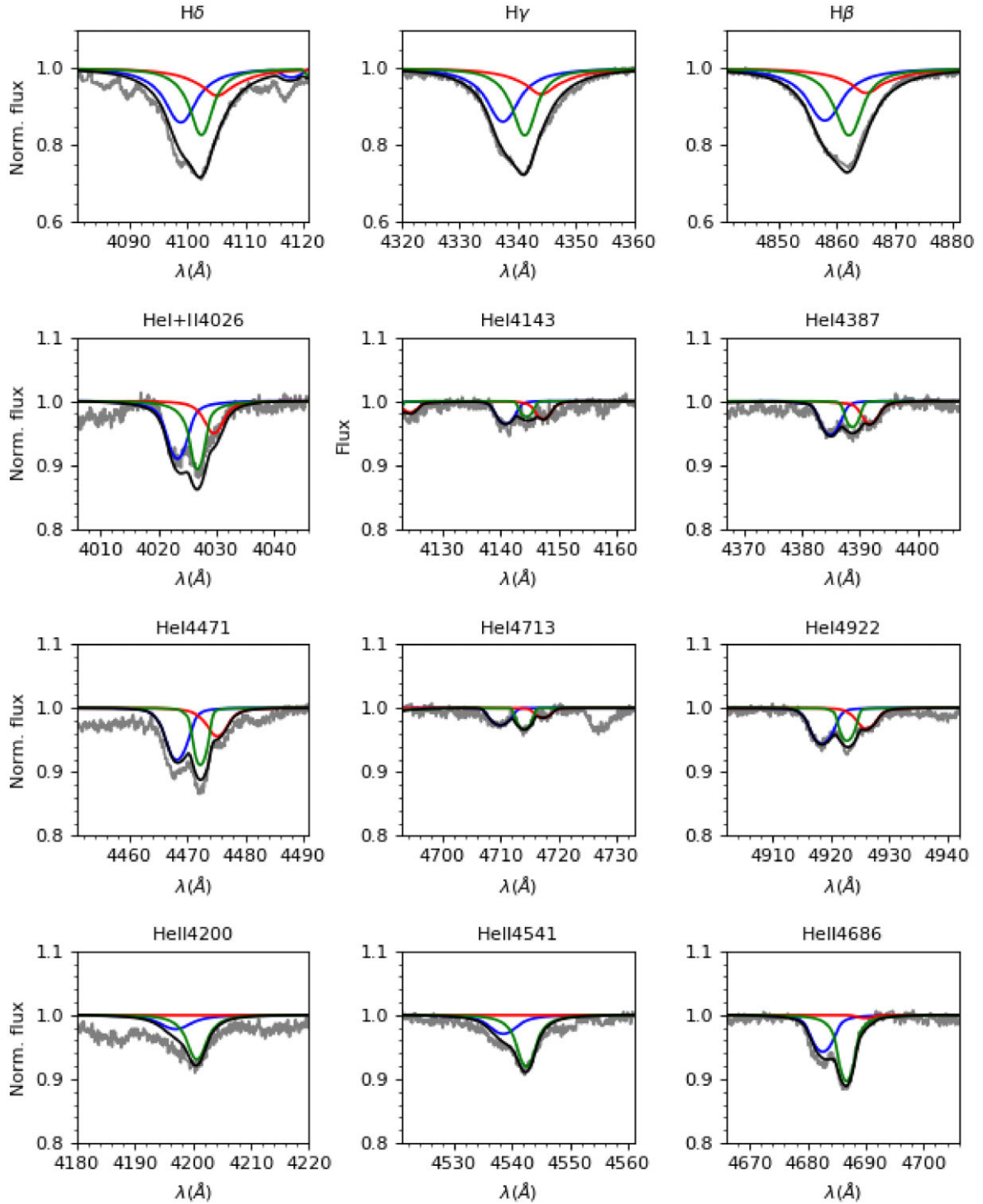


**Figure 5.** Observed FEROS spectrum compared to individual and combined synthetic models from the analysis with IACOB-GBAT. The best-fitting FASTWIND models for the individual components were added to obtain the combined spectrum.

On the contrary, the mechanisms associated with the formation of close binaries, i.e. fragmentation into an initially wider binary followed by the orbital decay of the protostars, are thought to produce coeval components. Some simple models for the formation of close solar-type binaries and compact triples (e.g. Moe & Kratter 2018; Tokovinin & Moe 2020) suggest that most of them form by disc fragmentation followed by accretion-driven inward migration.

Simon & Toraskar (2017) determined precise ages for the individual components in six low-mass young eclipsing binaries and found coevality within 0.3 Myr in five of them. Only one system showed an age difference of  $\sim 2.7$  Myr and, according to these authors, should be reconsidered.

Given the much shorter time-scales involved, the exact processes that lead to the formation of more massive binaries may differ with

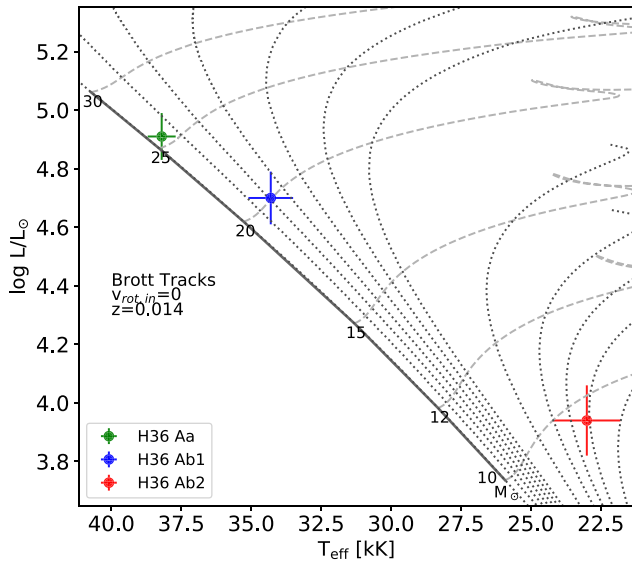


**Figure 6.** Location of the components of H36A in the HRD. Evolutionary tracks and isochrones from Brott et al. (2011) are shown. The ZAMS is indicated by the bold line and isochrones for  $\tau = 1, 2, 3, 4, 5, 6, 10, 13, 15, 17,$  and  $20$  Myr are also included. The vertical bar for each star represents the range in luminosity due to the uncertainty in the absolute magnitude.

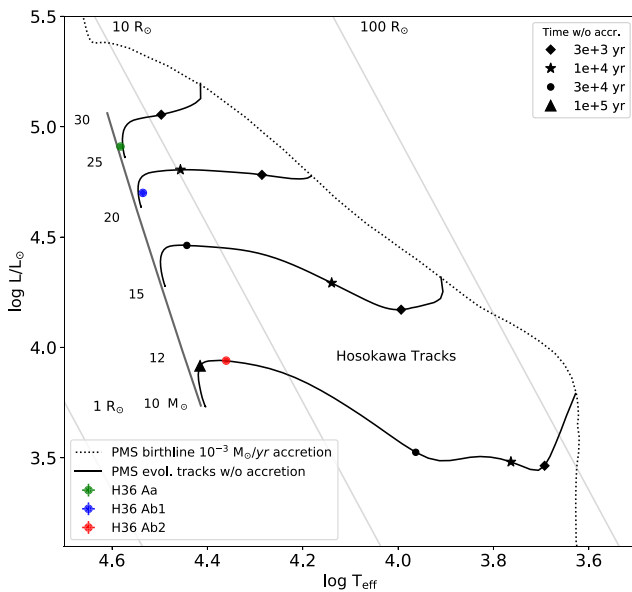


**Figure 7.** Same as Fig. 6, but using the evolutionary tracks of massive PMS stars from Hosokawa & Omukai (2009). An accretion rate of  $\dot{M} = 10^{-3} M_{\odot} \text{ yr}^{-1}$  was assumed. The dotted line represents the birthline at this accretion rate. The solid lines correspond to the evolutionary tracks after the star has finished accretion. The ZAMS from Ekström et al. (2012) and lines of constant stellar radius are also shown.

respect to the low-mass regime. However, the formation of close massive binaries is also believed to occur by disc fragmentation and accretion (Bonnell & Bate 1994). Recent numerical simulations show the viability of this channel for the formation of massive short-period binaries (Meyer et al. 2018). In this context, the formation of the inner binary components (and probably that of the outer star too) must proceed simultaneously, and hence they are expected to be coeval.

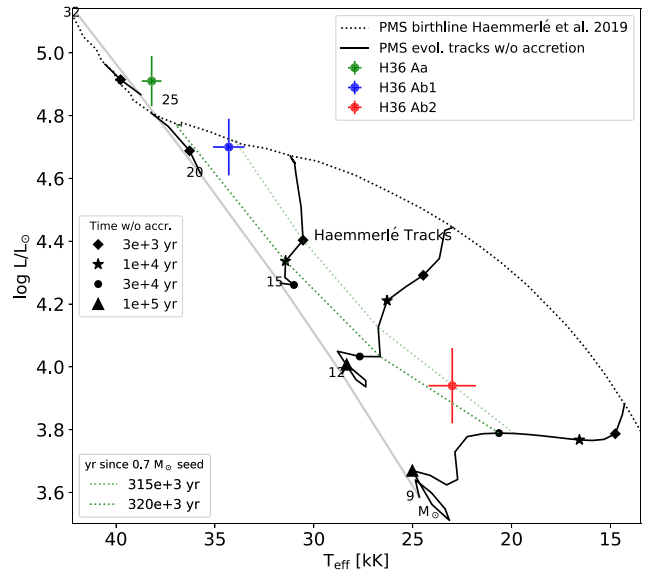


**Figure 8.** Same as Fig. 7, but using the PMS evolutionary tracks from Haemmerlé et al. (2019). The dotted line represents the birthline and the solid lines correspond to the evolutionary tracks after the star has finished accretion. The ZAMS from Ekström et al. (2012) is also shown, along with isochrones computed from the formation of the mass seed used in the models ( $0.7 M_{\odot}$ , see text).

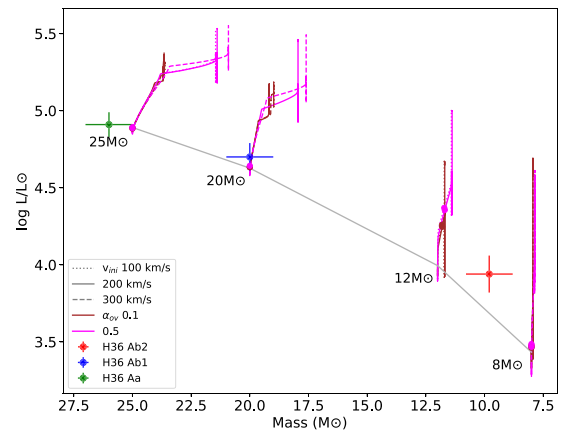


**Figure 9.**  $M-L$  plane showing the evolutionary tracks from Higgins & Vink (2019), for initial stellar masses ranging from  $8$  to  $25 M_{\odot}$  and initial rotational velocities ( $v_{ini}$ ) of  $100, 200,$  and  $300 \text{ km s}^{-1}$ . Two overshooting values are considered ( $\alpha_{ov} = 0.1$  and  $\alpha_{ov} = 0.5$ ). The thin line represents the ZAMS. The crosses indicate the positions of the three components of the H36A system. The small circles on the evolutionary tracks correspond to the observed effective temperatures ( $T_{eff}$ ) of each component. The best age estimate corresponds to the model age at which  $T_{eff}$ ,  $M$ , and  $L$  are reached at the same point.

How can we explain the non-coevality inferred from Fig. 6? A hypothesis is that the MS tracks are not representative of the evolutionary stage of H36A. Contrary to the classical paradigm which states that all massive stars arrive on the MS while still accreting deeply embedded within their natal molecular clouds, PMS models at high accretion rates show that, at the end of the accretion phase, stars as massive as  $25 M_{\odot}$  have not yet arrived at the ZAMS (Hosokawa & Omukai 2009; Haemmerlé et al. 2019). While massive protostars during the main accretion phase are very hard to observe, PMS

stars just after this phase have lost their thick envelopes and may be optically visible. As mentioned in the Introduction, although the new paradigm allows the existence of optically observable O-type stars in the last stages of their PMS evolution, their detection is limited by the small number of O stars and, more importantly, by the very short duration of the KH contraction phase.<sup>5</sup>

We explored the hypothesis of H36A being a PMS O system in contraction towards the ZAMS by using the theoretical models for massive PMS evolution by Hosokawa & Omukai (2009) and Haemmerlé et al. (2019). The results, illustrated in Figs 7 and 8, respectively, show the hypothesis is plausible. While the most massive component Aa is located just on the ZAMS, the positions of the close-binary components (Ab1 and Ab2) are consistent with massive objects in the last part of the KH contraction phase. None of the three stars is accreting anymore. Observationally, this is consistent with the appearance of the optical spectrum of H36A, which lacks any signs of active accretion, like inverse P Cygni profiles or strong emission in the Balmer lines (Arias et al. 2010). As the accretion has ceased, their final ZAMS masses should be equal to the current ones, which is verified by the agreement between the mass of the representative tracks and the values derived from the dynamics of the triple system (Sanchez-Bermudez et al. 2022).

In Section 3.4, the time elapsed from the end of accretion, as well as the time left to reach the ZAMS, were estimated for each component of H36A. In all cases, the duration of the whole KH contraction phase is very short, of the order a few thousand years for the most massive star, and shorter than  $80 \times 10^3$  yr for the close binary. The PMS models by Haemmerlé et al. (2019) allow further insight into the ages of these objects. Based on their location in the HRD, ages between  $315 \pm 100 \times 10^3$  and  $320 \pm 100 \times 10^3$  yr old were inferred for the components of H36A. The coincidence of ages among the three stars is interesting. An age younger than  $400 \times 10^3$  yr is also consistent with what it is expected for the Hourglass region.

#### 4.2 A note on the chemical composition

While the helium abundances determined for the components of H36A are fully compatible with baseline values, Ab1 and Ab2 exhibit central values slightly higher than those of the Aa component. However, compared to the helium measurements in a large sample of Galactic O stars performed by Holgado (2019), these values are standard values. A further insight pertains to the observed helium abundance  $Y_{\text{He}}$  in O stars compared to model predictions. While some of the most widely used single-star evolutionary models for massive stars, including those utilized by BONNSAI (Brott et al. 2011), suggest no alteration of  $Y_{\text{He}}$  on the surface of O stars during the MS, the empirical analysis by Holgado (2019) reveals a discrepancy with these predictions, highlighting a departure from theoretical expectations. The observed discrepancy raises questions about a potential missing ingredient in the current models, such as binarity or disparate initial abundances. Many observed helium determinations are not entirely explainable by most current models. Thus, although the helium measurements for Ab1 and Ab2 show a slight overabundance, we believe this discrepancy should not overshadow the broader observation that all three stars in the system do not conform to an MS model isochrone and, notably, they can be effectively adjusted and share a similar age when using PMS models.

<sup>5</sup>For example,  $t_{\text{KH}} \approx 4 \times 10^4$  yr for stars with masses  $\sim 20 M_{\odot}$  accreting at a rate of  $\dot{M}_* = 10^{-3} M_{\odot} \text{ yr}^{-1}$  (Davies et al. 2011).

## 5 SUMMARY AND CONCLUSIONS

This paper is the second part of a detailed spectroscopic study devoted to the massive triple system H36A. This object was historically pointed out as an extremely young star, likely still on the ZAMS, although its evolutionary status had never been deeply explored before. Here, we took advantage of the individual spectra of the three components recovered through a disentangling method in Paper I to investigate the physical and evolutionary properties of the system.

A quantitative spectroscopic analysis using FASTWIND stellar atmosphere models was performed on these spectra to determine the photospheric and wind parameters of each component. Their radii and luminosities were also determined and they were placed in the HRD. We used both MS and PMS evolutionary models to derive the evolutionary masses and ages of the stellar components, given the extremely young age of Herschel 36 and the Hourglass Nebula proposed on the basis of different observational studies.

While evolutionary masses are more or less similar independently of the set of models used, the inferred ages greatly differ and, consequently, they can be useful for distinguishing the current stage of the system's evolution. MS tracks lead to too advanced ages for the components of the inner binary of H36A (Ab1, Ab2) and, importantly, to an age discrepancy between them that is difficult to explain within the current scenarios for the formation of such close pairs. The age difference between Ab1 and Ab2 exceeds 12 Myr, which is significantly greater than the systematic uncertainties associated with using models that assume a default mixing efficiency.

The age discrepancy among the components of H36A could be resolved by considering that the system is in the final stages of the PMS phase, with the inner binary components still contracting towards the ZAMS and expected to reach it within a few tens of thousands of years. The most massive component, Aa, is positioned virtually on the ZAMS, indicating that it may be slightly more evolved, which is consistent with its greater mass. We note that the helium abundances determined for the inner components of H36A are slightly higher than expected for PMS objects, though still within the range of baseline values. This indicates that the possibility of the stars being on the MS cannot be entirely ruled out.

This study highlights the importance of considering multiple evolutionary models to comprehensively understand complex systems like H36A. We acknowledge that the models utilized in this study to infer the PMS ages of the stellar components were not specifically tailored for the formation of a hierarchical triple system like H36A. Nevertheless, given the current limitations imposed by the available models, the hypothesis of H36A being a massive PMS system appears plausible. This hypothesis will have to be reassessed and validated once comprehensive models for the evolution of massive PMS systems are developed. In any case, this study shows that H36A is an interesting candidate for a massive star that has not yet reached the MS, making it a key object for understanding massive star formation and early evolution.

## ACKNOWLEDGEMENTS

Dedicated to Rodolfo ‘Osito’ Barbá, from whom the first author learned about astronomy and life more than she could have learned anywhere else. We would like to thank the reviewers for their detailed reviews and constructive comments, which have helped us improve the manuscript. JIA acknowledges the financial support from the Dirección de Investigación y Desarrollo de la Universidad de La Serena (ULS), through the project PR2324063. GH acknowledges support from the State Research Agency (AEI) of

the Spanish Ministry of Science and Innovation (MICINN) and the European Regional Development Fund, FEDER under grants LOS MÚLTIPLES CANALES DE EVOLUCIÓN TEMPRANA DE LAS ESTRELLAS MASIVAS/ LA ESTRUCTURA DE LA VIA LACTEA DESVELADA POR SUS ESTRELLAS MASIVAS with reference PID2021-122397NB-C21/PID2022-136640NB-C22/10.13039/501100011033. RG acknowledges support from grant PICT 2019-0344. We want to thank Alba Casasbuenas for her helpful advice that improved this manuscript significantly.

## DATA AVAILABILITY

The data underlying this article will be shared on reasonable request to the corresponding author.

## REFERENCES

- Arias J. I. et al., 2010, *ApJ*, 710, L30  
 Arias J. I. et al., 2016, *AJ*, 152, 31  
 Arias J. I., Barbá R. H., Maíz Apellániz J., Morrell N. I., Rubio M., 2006, *MNRAS*, 366, 739  
 Arias J. I., Barbá R. H., Morrell N. I., 2007, *MNRAS*, 374, 1253  
 Barbá R. H., Gamen R., Arias J. I., Morrell N. I., 2017, in Eldridge J. J., Bray J. C., McClelland L. A. S., Xiao L., eds, *Proc. IAU Symp. 329, The Lives and Death-Throes of Massive Stars*. Kluwer, Dordrecht, p. 89  
 Barbá R. H., Gamen R., Arias J. I., Morrell N., Maíz Apellániz J., Alfaro E., Walborn N., Sota A., 2010, in Rivinius TH., Curé M., eds, *Revista Mexicana de Astronomía y Astrofísica Conference Series, Vol. 38*. p.30  
 Behrend R., Maeder A., 2001, *A&A*, 373, 190  
 Bonnell I. A., Bate M. R., 1994, *MNRAS*, 271, 999  
 Brott I. et al., 2011, *A&A*, 530, A115  
 Campillay A. R., Arias J. I., Barbá R. H., Morrell N. I., Gamen R. C., Maíz Apellániz J., 2019, *MNRAS*, 484, 2137  
 Chakraborty A., Anandarao B. G., 1997, *AJ*, 114, 1576  
 Clarke, C. J., Bonnell I. A., 2008, *MNRAS*, 388, 1171  
 Damiani F., Flaccomio E., Micela G., Sciortino S., Harnden F. R. J., Murray S. S., 2004, *ApJ*, 608, 781  
 Davies B., Hoare M. G., Lumsden S. L., Hosokawa T., Oudmaijer R. D., Urquhart J. S., Mottram J. C., Stead J., 2011, *MNRAS*, 416, 972  
 Ekström S. et al., 2012, *A&A*, 537, A146  
 González J. F., Levato H., 2006, *A&A*, 448, 283  
 Haemmerlé L. et al., 2019, *A&A*, 624, A137  
 Higgins E. R., Vink J. S., 2019, *A&A*, 622, A50  
 Higgins E. R., Vink J. S., 2023, *MNRAS*, 518, 1158  
 Holgado G. et al., 2018, *A&A*, 613, A65  
 Holgado G. et al., 2020, *A&A*, 638, A157  
 Holgado G., 2019, PhD thesis, [University of La Laguna](https://www.researchgate.net/publication/354844444)  
 Holgado G., Simón-Díaz S., Herrero A., Barbá R. H., 2022, *A&A*, 665, A150  
 Hosokawa T., Omukai K., 2009, *ApJ*, 691, 823  
 Kratter K. M., 2012, in Drissen L., Robert C., St-Louis N., Moffat A. F. J., eds, *ASP Conf. Ser. Vol. 465, Proceedings of a Scientific Meeting in Honor of Anthony F. J. Moffat*. Astron. Soc. Pac., San Francisco, p. 451  
 Kratter K. M., Matzner C. D., Krumholz M. R., 2008, *ApJ*, 681, 375  
 Kratter K. M., Matzner C. D., Krumholz M. R., Klein R. I., 2010, *ApJ*, 708, 1585  
 Krumholz M. R. 2015 <https://arxiv.org/pdf/1511.03457>  
 Kuiper R., Hosokawa T. 2018, *A&A*, 616, A101  
 Kuiper R., Yorke H. W. 2013, *ApJ*, 772, 61  
 Lada C. J., Gull T. R., Gottlieb C. A., Gottlieb E. W., 1976, *ApJ*, 203, 159  
 Maíz Apellániz J., Barbá R. H., Fernández Aranda R., Pantaleoni González M., Crespo Bellido P., Sota A., Alfaro E. J., 2022, *A&A*, 657, A131  
 Martins F., Schaerer D., Hillier D. J., 2005, *A&A*, 436, 1049  
 Meyer D. M. A., Kuiper R., Kley W., Johnston K. G., Vorobyov E., 2018, *MNRAS*, 473, 3615  
 Moe M., Kratter K. M., 2018, *ApJ*, 854, 44  
 Moeckel N., Clarke C. J. 2011, *MNRAS*, 410, 2799  
 Ochsendorf B. B., Ellerbroek L. E., Chini R., Hartoog O. E., Hoffmeister V., Waters L. B. F. M., Kaper L., 2011, *A&A*, 536, L1  
 Palau A., Sánchez Contreras C., Sahai R., Sánchez-Monge Á., Rizzo J. R., 2013, *MNRAS*, 428, 1537  
 Prisinzano L. et al., 2019, *A&A*, 623, A159  
 Puls J., Urbaneja M. A., Venero R., Repolust T., Springmann U., Jokuthy A., Mokiem M. R., 2005, *A&A*, 435, 669  
 Repolust T., Puls J., Herrero A., 2004, *A&A*, 415, 349  
 Sabín-Sanjulián C. et al., 2014, *A&A*, 564, A39  
 Sanchez-Bermudez J. et al., 2022, *MNRAS*, 514, 1162  
 Santolaya-Rey A. E., Puls J., Herrero A., 1997, *A&A*, 323, 488  
 Schneider F. R. N., Langer N., de Koter A., Brott I., Izzard R. G., Lau H. H. B., 2014, *A&A*, 570, A66  
 Schneider F. R. N. et al. 2018, *Science*, 359, 69  
 Schootemeijer A. et al., 2021, *A&A*, 646, A106  
 Simon M., Toraskar J., 2017, *ApJ*, 841, 95  
 Simón-Díaz S., Castro N., Herrero A., Puls J., Garcia M., Sabín-Sanjulián C., 2011, *J. Phys.: Conf. Ser.*, 328, 012021  
 Simón-Díaz S., Herrero A., 2014, *A&A*, 562, A135  
 Simón-Díaz S., Herrero A., Sabín-Sanjulián C., Najarro F., Garcia M., Puls J., Castro N., Evans C. J., 2014, *A&A*, 570, L6  
 Tokovinin A., Moe M., 2020, *MNRAS*, 491, 5158  
 Walborn N. R., 2009, in Livio M., Villaver E., eds, *Massive Stars: From Pop III and GRBs to the Milky Way*. Space Telescope Science Institute Symposium Series No. 20. Cambridge Univ. Press, Cambridge, p. 167  
 Yorke H. W., 1986, *ARA&A*, 24, 49  
 Zhang Y. et al., 2019, *Nat. Astron.*, 3, 517

This paper has been typeset from a  $\text{\TeX}/\text{\LaTeX}$  file prepared by the author.